Renewable and Sustainable Energy Reviews 203 (2024) 114747

Contents lists available at ScienceDirect

Renewable and Sustainable Energy Reviews

journal homepage: www.elsevier.com/locate/rser

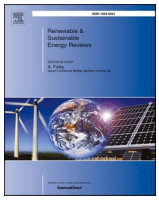

Impact of global warming on wind power potential over East Asia

Changyong Park [a], Seok-Woo Shin [a], Dong-Hyun Cha [a,*], Seung-Ki Min [b], Young-Hwa Byun [c], Jin-Uk Kim [c], Youngeun Choi [d]

[a] Department of Civil, Urban, Earth, and Environmental Engineering, Ulsan National Institute of Science and Technology, 44919, Republic of Korea
[b] Division of Environmental Science and Engineering, Pohang University of Science and Technology, 37673, Republic of Korea
[c] National Institute of Meteorological Sciences, 63568, Republic of Korea
[d] Department of Geography, Konkuk University, 05029, Republic of Korea

ARTICLE INFO

Keywords:
Wind power potential
Renewable energy
Regional climate models
Carbon emission scenario
Coordinated regional downscaling
Experiment–East Asia
Future projection

ABSTRACT

Wind power, which is the fastest–growing renewable energy source, is directly influenced by weather or climate conditions. This study examined the recent changes and future projections under different carbon emission levels in the wind power potential (Wpot) over East Asia using the ERA5 datasets and high–resolution multiple regional climate models (RCMs). Because wind conditions are constantly changing, we employed the wind velocity range–based approach for estimating the Wpot using the shortest time interval data available, which is the three–hourly wind velocity. Seasonal Wpot climatology of area–averaged Wpot over East Asia was the highest in spring. The average Wpot showed the highest values in northern China and southern Mongolia throughout all seasons, while recent changes in the Wpot over East Asia were characterized by overall increases in spring, autumn, and winter, but a decrease in summer. However, there were large regional variabilities. Northern China and southern Mongolia are expected to remain significant regions with high Wpot in the future. This is due to the large contribution of the frequency of optimal wind conditions, ranging from 12 m s^{-1} to 25 m s^{-1}, to the Wpot in these regions, both currently and in the future. The average future Wpot in East Asia is expected to show no significant changes in both the low and the highest carbon emission scenarios compared to the present. However, it is projected that regional disparities in the Wpot will increase in a scenario with enhanced emission by the end of the 21st century.

Nomenclature. Abbreviation

BAU	Business as usual
CCLM	Consortium for small–scale modeling regional climate model
CMIP5	Coupled model intercomparison project 5
CORDEX	Coordinated regional climate downscaling experiment
DRE	Distributed renewable energy
ERA5	European Centre for medium–range weather forecasts reanalysis 5
GCM	Global climate model
GHG	Greenhouse gas
HadGEM2–AO	Hadley Centre global environment model version 2-atm–ocean
HadGEM3–RA	Hadley Centre global environment model version 3–regional climate model
JPN	Japan
JULES	Joint UK land environment simulator
KOR	Korea
MME	Multi–model ensemble
MPI–ESM–LR	Max Planck Institute–earth system model–low resolution
NC	North China

(*continued on next column*)

(*continued*)

NCAR CCM2	National Center for atmospheric research community climate model 2
NCAR CLM3	National Center for atmospheric research community land model 3
NEC	Northeast China
NWC	Northwest China
PVpot	Photovoltaic power potential
RCM	Regional climate model
RCP	Representative concentration pathways
RE100	Renewable electricity 100
SC	South China
SNURCM	Seoul National University regional climate model
WCRP	World climate research programme
Wpot	Wind power potential
YHR	Yangtze–Huaihe River Basin
Symbols	
T_1	Period from 2041 to 2065
T_2	Period from 2075 to 2099
V_O	Cut–out velocity

(*continued on next page*)

* Corresponding author.
E-mail address: dhcha@unist.ac.kr (D.-H. Cha).

https://doi.org/10.1016/j.rser.2024.114747
Received 26 September 2023; Received in revised form 18 June 2024; Accepted 12 July 2024
Available online 18 July 2024

(*continued*)

$V1$	Range from 0 to 3.5 m s^{-1}
$V2$	Range from 3.5 m s^{-1} to 12 m s^{-1}
$V3$	Range from 12 m s^{-1} to 25 m s^{-1}
$V4$	Above 25 m s^{-1}
$V(h)$	Wind velocity at the turbine hub height
$V(h_0)$	Wind velocity at 10 m height
V_I	Cut–in velocity
V_R	Rated velocity

1. Introduction

Various international efforts are currently underway to restrain global warming and reduce carbon emissions, including initiatives such as the Paris Agreement and RE100 (Renewable Electricity 100). In particular, although RE100 is not a binding international agreement between countries, it aims to encourage companies to voluntarily increase their use of renewable energy sources. East Asia is a densely populated and highly industrialized region responsible for the world's highest level of greenhouse gas (GHG) emissions due to its extensive use of fossil fuels. Therefore, to reduce GHG emissions, it is necessary to significantly increase the proportion of renewable energy in both energy production and industrial activities in this region. In 2021, China contributed 40 % of the global increase in wind energy compared to 2020 due to a significant increase in wind power capacity [1]. Furthermore, several enterprises in the three major East Asian countries (China, Japan, and South Korea) are making efforts, including joining RE100. However, these efforts are still insufficient, and to address this issue, RE100 encourages renewable energy production and urges companies to increase their use of renewable energy [2].

Wind power is the fastest–growing renewable energy source [3]. In recent years, wind turbines have been widely installed not only onshore but also offshore. As a result, many industrial complexes located near the coast of East Asia can utilize efficiently transmitted electricity generated from nearby offshore wind farms. This leads to creating of a favorable condition for companies in terms of their alignment with the RE100 initiative. In contrast to traditional centralized energy systems that require large–scale power plants and extensive transmission lines, a distinguishing feature of decentralized energy systems, known as distributed energy systems, is the placement of energy generation facilities closer to the point of energy consumption. This approach has gained significant attention in recent years due to its potential to reduce inefficiencies in transmission and distribution, as well as associated economic and environmental costs. Renewable energy, such as wind power production in offshore mentioned earlier, aligns exceptionally well with the concept of distributed energy systems. Integrating renewable energy into distributed energy systems, known as Distributed Renewable Energy (DRE), provides environmentally, socially, and economically sustainable energy [4].

To ensure the efficient production of renewable energy and develop reliable policies for future renewable energy production, a detailed spatiotemporal investigation of the current and future changes in the potential for renewable energy production is required. The Coordinated Regional Climate Downscaling Experiment (CORDEX) project established through sponsorship by the World Climate Research Programme (WCRP), which produces spatially detailed regional climate models for 14 regional domains across the globe, is currently being carried out by numerous universities and research institutions. This project aims to overcome the limitations of global climate models (GCMs) with low spatial resolution and provide quality–controlled climate information at regional and local scales through dynamically downscaled techniques [5]. The high–resolution regional climate models (RCMs) produced through this project are being applied in various fields for climate change impact assessment. In recent years, there has been an increasing number of studies on renewable energy in the East Asia region concerning this topic, specifically focusing on the future potential projection of wind [6–12] and photovoltaic [13–16] energy production using RCMs. Many of these studies have been centered around China. Park et al. [13] recently investigated the current and future changes in East Asia's photovoltaic power potential (PVpot) using the RCMs produced through the CORDEX–East Asia project. As a follow–up to Park et al. [13], this study investigated the recent changes and future projections under different carbon emission levels in the wind power potential (Wpot) over East Asia land domain, which includes China, the Korean Peninsula, Japan, and parts of Mongolia and Russia, using the ERA5 (European Centre for Medium–Range Weather Forecasts reanalysis 5) datasets and high–resolution multi–RCMs participating in the CORDEX–East Asia phase II project. Furthermore, because wind conditions are constantly changing, we employed the wind velocity range–based approach for estimating the Wpot using the shortest time interval data available, which is the three–hourly wind velocity data. Since the wind power output does not have a linear relationship with wind velocity and varies depending on the wind velocity ranges, a detailed analysis of each wind velocity range is required to estimate Wpot. In this study, the current changes and future projections of Wpot were presented in detail according to the wind velocity ranges, and the contribution of each wind velocity range to Wpot was also estimated. Furthermore, a multi–model ensemble was constructed to reduce uncertainty using various RCMs, and multi–scenarios were applied to estimate Wpot according to carbon emission levels. It was determined that applying all of these factors to East Asian Wpot estimates would lead to more reliable results.

The remainder of this paper is organized as follows. The observational dataset, regional climate models, and analysis methods are introduced in Section 2. The observed seasonal climatology for the wind power potential and its recent change and the future changes of wind power potential using the RCMs produced through the CORDEX–East Asia phase II project over East Asia are investigated in Section 3. Finally, a summary and discussion are presented in Section 4.

2. Data and methods

2.1. Observational data and models

The land regions of East Asia (80°E−150°E and 20°N–50°N) were selected as the analysis domain, which includes China (except for the western arid region), the Korean peninsula, Japan, and parts of Mongolia and Russia. The primary variable for observational data and models used in this study is three–hourly 10 m wind velocity. In this study, wind velocity data with a 3-h interval, the shortest one in the RCMs produced, was used to reflect the wind characteristics as much as possible, which change every moment throughout the day. The recent changes and future projections for wind velocity and Wpot were assessed seasonally: spring (March–April–May), summer (June–July–August), autumn (September–October–November), and winter (December–January–February).

The ERA5 datasets with a horizontal resolution of 0.25° × 0.25° covering the period from 1979 to 2018 were employed to examine the recent changes in Wpot and evaluate the performance of the RCMs. It has been reported that the ERA5 dataset has considerably improved in many physical configurations or schemes compared to previously produced ERA–Interim datasets [17]. However, while ERA5 datasets exhibit high performance in reproducing near–surface wind climatology in China, they have limitations in capturing long–term trends effectively [18,19].

The future change in Wpot over East Asia was estimated using the six RCM simulations with 25–km horizontal resolution forced by two CMIP5 (Coupled Model Intercomparison Project 5) GCMs, HadGEM2–AO (Hadley Centre global environment model version 2-atm–ocean) and MPI–ESM–LR (Max Planck Institute–earth system model–low resolution), participating in the CORDEX–East Asia phase II project. Here, it is known that HadGEM2–AO and MPI–ESM–LR GCMs

Table 1
Configurations of RCMs used in this study.

Configuration \Model	HadGEM3–RA (Hadley Centre global Environment model version 3 regional climate model)	SNURCM (Seoul National University regional climate model)	CCLM (Consortium for small–scale modeling (COSMO) climate limited–area modeling)
GCMs	HadGEM2–AO and MPI–ESM–LR	HadGEM2–AO and MPI–ESM–LR	HadGEM2–AO and MPI–ESM–LR
Number of grid points (latitude × longitude)	251 × 396	260 × 405	251 × 396
Vertical levels	63 eta	σ–24	Hybrid–40
Dynamic framework	Non–hydrostatic	Non–hydrostatic	Non–hydrostatic
Convection scheme	Revised mass flux	Kain–Fritch II	Tiedtke
Microphysics	Single moment bulk	Reisner II	Extended DM
Radiation	General 2–stream radiation [24,25]	NCAR CCM2 (National Center for atmospheric research community climate model 2) package [26,27]	Ritter and Geleyn [28]
Land surface model	Joint UK Land Environment Simulator (JULES)	NCAR CLM3 (National Center for atmospheric research community land model 3)	TERRA ML
References	Davis et al. [29]	Cha and Lee [30]	Rockel et al. [31]

better simulate the observed East Asian climate compared to other CMIP5 GCMs [20–23]. Table 1 presents the model configurations of six RCM simulations with different physical schemes. The *Historical* experiment was used to evaluate the RCM's performance during the 25 years from 1981 to 2005. To investigate and compare the future projection of Wpot in response to the carbon emission levels over East Asia, two scenarios of *RCP (Representative concentration pathways) 2.6* and *RCP8.5* were applied for two future periods (2041–2065 and 2075–2099). The *RCP2.6* is the scenario with low carbon emissions that most closely corresponds to the *Paris Agreement*, and the *RCP8.5* is the *business as usual* (BAU) scenario with the highest carbon emissions. To reduce the uncertainty between RCMs arising from different model configurations, a multi–model ensemble (MME) was constructed by equally weighted averages of six RCMs. All RCM outputs underwent a post–processing step of interpolating into 0.25° × 0.25° grids of the ERA5 spatial resolution using the bilinear interpolation method.

2.2. Analysis methods

As stated in section 2.1, 10 m wind speed data was applied for both observation and future scenarios. Since the turbine hub height is typically installed from 60 m to 100 m above the ground [32], extrapolation of wind velocity data, such as Eq. (1) [33,34], should be performed before calculating Wpot.

$$V(h) = V(h_0)\left(\frac{h}{h_0}\right)^{1/7} \tag{1}$$

where $V(h)$ denotes the wind velocity at the turbine hub height and 90 m was applied according to Ref. [34]. $V(h_0)$ represents the wind velocity at 10 m height.

In this study, the Wpot was estimated using the wind power curve presented by Mathew (2006) [35]. The wind power curve categorizes four wind velocity ranges with distinct characteristics, and the power performance of each range can be expressed as Eq. (2). Several recent studies focusing on the European regions have utilized this as an indicator to estimate wind power potential [34–39]. The wind velocity range–based Wpot estimation equation and its explanation are as follows.

$$Wpot = \begin{cases} 0 & if\ V < V_I \\ \dfrac{V^3 - V_I^3}{V_R^3 - V_I^3} & if\ V_I \le V < V_R \\ 1 & if\ V_R \le V < V_0 \\ 0 & if\ V \ge V_0 \end{cases} \tag{2}$$

Here, the Wpot is a dimensionless magnitude. Although the value may vary depending on the type of wind turbine, a wind turbine has three important wind velocity values: cut–in velocity (V_I), rated velocity

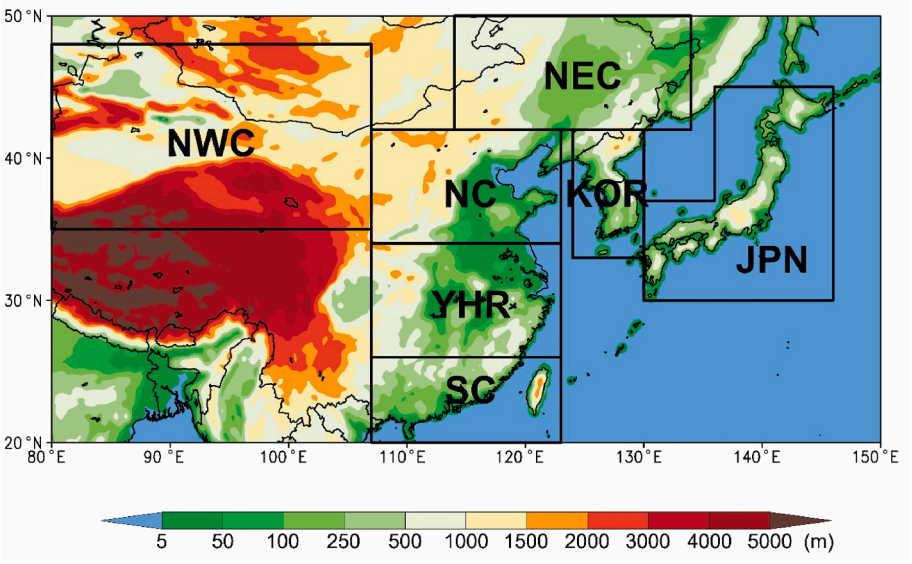

Fig. 1. Analysis domain and seven sub–regions over East Asia: Northwest China (NWC), Northeast China (NEC), North China (NC), Yangtze–Huaihe River Basin (YHR), South China (SC), Korean peninsula (KOR), and Japan (JPN). Each color indicates altitude (unit: m).

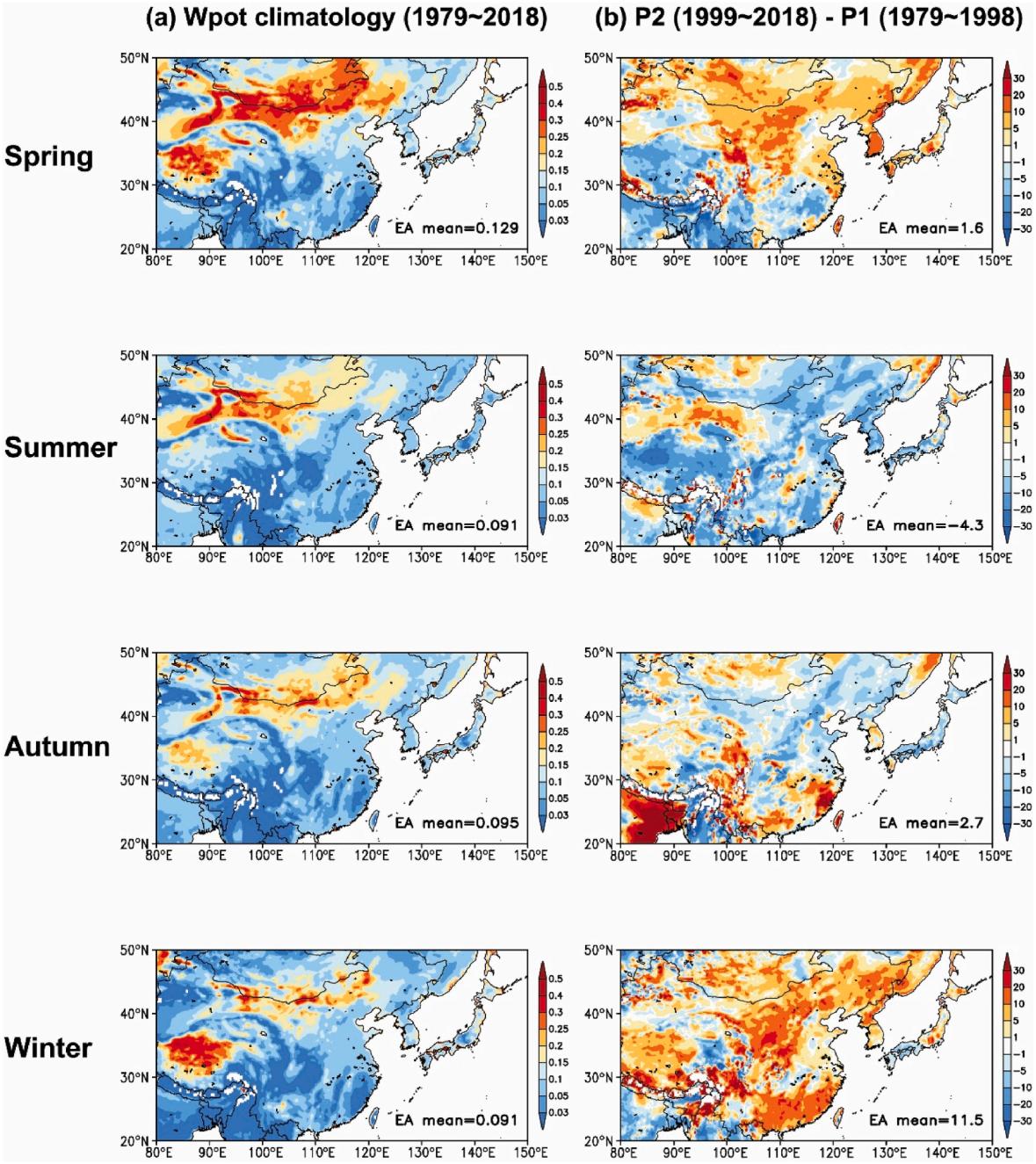

Fig. 2. Spatial distributions of (a) observed seasonal mean for the Wpot (no unit) and (b) the difference (unit: %) between the second half (1999–2018) and the first half (1979–1998) of the past 40 years (1979–2018) over East Asia. Area mean values are given in the bottom right corners.

(V_R), and cut–out velocity (V_O) [32,35]. These three wind velocities are used as the references for calculating Wpot and Tobin et al.'s [34] criteria ($V_I = 3.5$ m s^{-1}, $V_R = 12$ m s^{-1}, $V_O = 25$ m s^{-1}) was applied in this study. The characteristics of power output and Wpot for each range between the reference velocities are as follows [32,35]. The V_I is the minimum wind velocity at which the system starts producing, and the Wpot from 0 m s^{-1} to V_I is zero. The V_R is the wind velocity at which rated power is reached, the maximum power output of the generator. In the wind velocity range from V_I to V_R, the power produced by the wind turbine increases as the wind velocity increases. Between V_R and V_O, since the turbine is constrained to produce a constant output corresponding to V_R regardless of velocity changes, the Wpot from V_R and V_O is expressed one. The V_O is defined as the maximum wind velocity at which the turbine can deliver power. At wind velocities exceeding V_O, Wpot becomes zero as the machine must come to a complete stop to protect the rotor and drive train from overload damage. Three–hourly Wpots were calculated for both observation and scenarios and then averaged seasonally over the periods. The future projection of the Wpot for two emission scenarios of *RCP2.6* and *RCP8.5* was expressed as a percent (%) change relative to the climatology of the *Historical* experiment. Seven sub–regions within the study domain were selected to examine the present distribution and future changes of Wpot in detail by region. The Korean peninsula and Japanese regions were added to the five sub–regions selected by Yu et al. [40] for China, resulting in a total of seven sub–regions as follows (Fig. 1). The locations and abbreviations of the sub–regions used in this study are presented in the list of abbreviations.

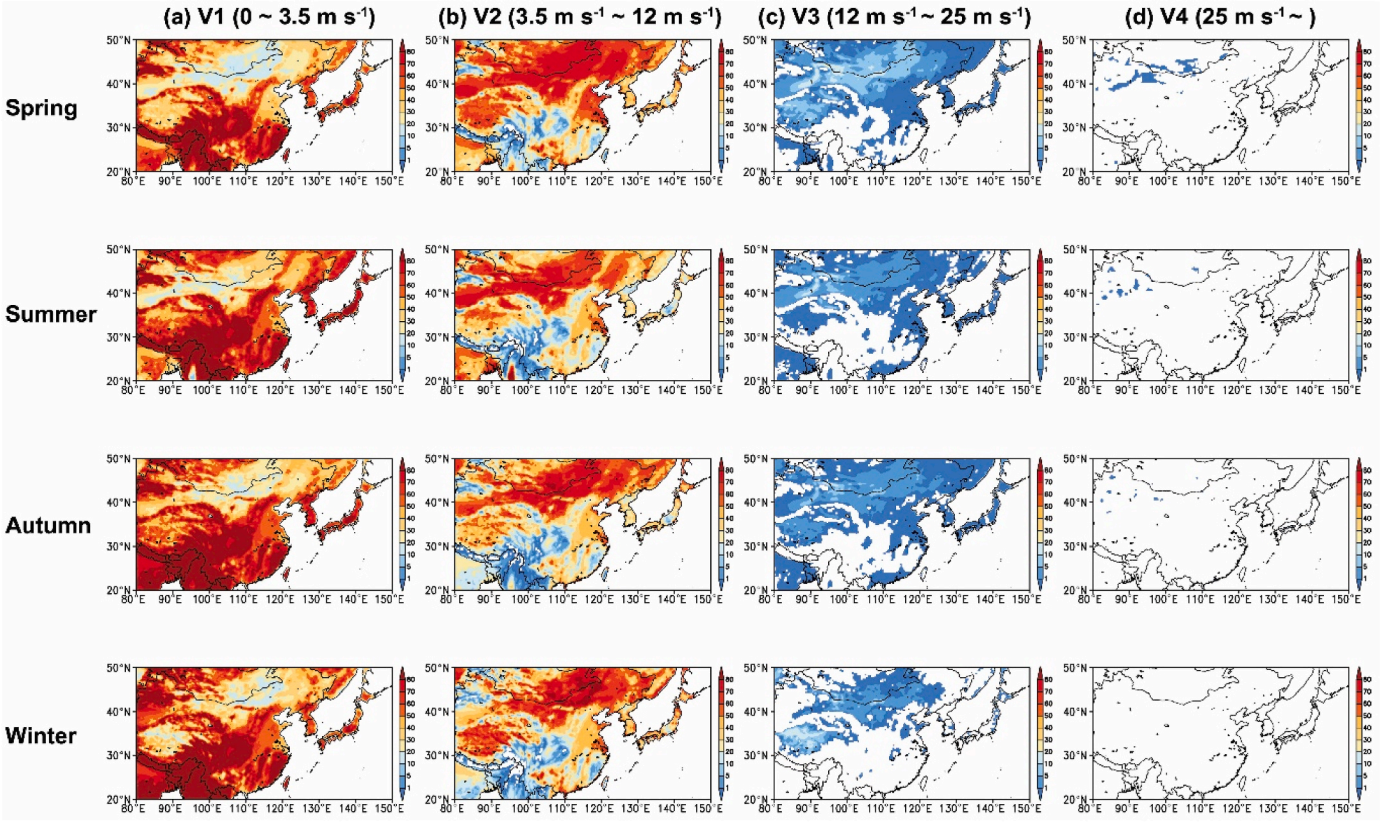

Fig. 3. The ratio (unit: %) of the frequency of each wind velocity range to the total frequency of ERA5 three–hourly wind velocity for the past 40 years (1979–2018) over East Asia. (a) ***V1*** range (0 – 3.5 m s^{-1}), (b) ***V2*** range (3.5 m s^{-1} – 12 m s^{-1}), (c) ***V3*** range (12 m s^{-1} – 25 m s^{-1}), and (d) ***V4*** range (25 m s^{-1} –).

3. Results

3.1. Observed mean for the wpot and RCM performances over East Asia

The spatial distribution of the observed seasonal climatology for the Wpot and its recent change (%) using the ERA5 dataset was investigated (Fig. 2). Seasonal Wpot climatology of area–averaged Wpot over East Asia was the highest in the spring, and the rest of the seasons were similar. The Wpot climatology was highest in northern China and southern Mongolia regions throughout all seasons. In the previous study by Park et al. [13], these regions have the highest PVpot for solar energy production, so it is a 'Hotspot' for renewable energy production. First, linear regression coefficients regarding the observed seasonal mean for the Wpot during the past 40 years (1979–2018) were investigated (Fig. S1). In the spring, the Wpot exhibited increasing trends at high latitudes and decreasing trends at low latitudes. For the summer, there was a trend of overall decrease. The autumn showed no notable change compared to the other three seasons, and the winter had increasing trends in most regions. As shown in Fig. 2(a), Wpot climatology within East Asia has large regional differences. So it would be appropriate to investigate the relative change of Wpot based on a percentage rather than the trend in analyzing the past Wpot change. Accordingly, to focus on recent changes, the difference between the second half (P2: 1999–2018) and the first half (P1: 1979–1998) of the past 40 years (1979–2018) was investigated as a percentage change to analyze the observed recent changes in the seasonal mean of the Wpot over East Asia (Fig. 2(b)). The recent changes in the seasonal mean of area–averaged Wpot over East Asia (See the value at the bottom right of each figure) did not show notable changes in spring, summer, and autumn, but its spatial distributions are large regional variabilities. On the other hand, the winter had a considerable increase of 11.5 %, and regionally, the increase was remarkable in the southern China region.

According to Eq. (2), in relation to the calculation of Wpot, the contribution of the four wind velocity ranges to the Wpot climatology of the past 40 years (1979–2018) differs for each range. Therefore, the ratio (%) of the frequency of each wind velocity range to the total frequency of ERA5 three–hourly wind velocity for the past 40 years over East Asia was investigated (Fig. 3). The proportion of the range from 0 to 3.5 m s^{-1} (hereafter *V*1 range) contributing zero values to Wpot generally showed a high proportion in the low latitudes and a low proportion in the high latitudes. In particular, during the spring when the Wpot is highest, the *V*1 range accounts for more than 80 % in the central and southeastern regions of China. In comparison, the northern China and southern Mongolia regions had a proportion of less than 20 %. On the other hand, the ranges of 3.5 m s^{-1} to 12 m s^{-1} (hereafter *V*2 range) and 12 m s^{-1} to 25 m s^{-1} (hereafter *V*3 range), which significantly contribute to the total Wpot, showed the opposite pattern to that of the *V*1 range. The regions with a high (low) proportion of the *V*1 range showed a low (high) proportion of the *V*2 and *V*3 ranges. Moreover, the *V*3 range, which is a good wind velocity range for the Wpot, had a lower proportion than the *V*2 range, accounting for less than 20 % of the total wind velocity frequency. In spring, the *V*3 range was hardly observed in the central and southeastern regions of China, while it accounted for up to 20 % of the total wind velocity frequency in northern China and southern Mongolia regions. Similar to the *V*1 range, the ranges above 25 m s^{-1} (hereafter *V*4 range) that contribute zero values to the Wpot were not observed in most regions of East Asia throughout all seasons, but in northeastern China and southern Mongolia regions in spring, it had a proportion of less than 1 % for the total wind velocity frequency. Therefore, the results of the proportional distribution of wind velocity ranges for the total wind velocity frequency led to the distribution patterns of the Wpot climatology shown in Fig. 2 (a).

The difference (%) in the frequency of each wind velocity range

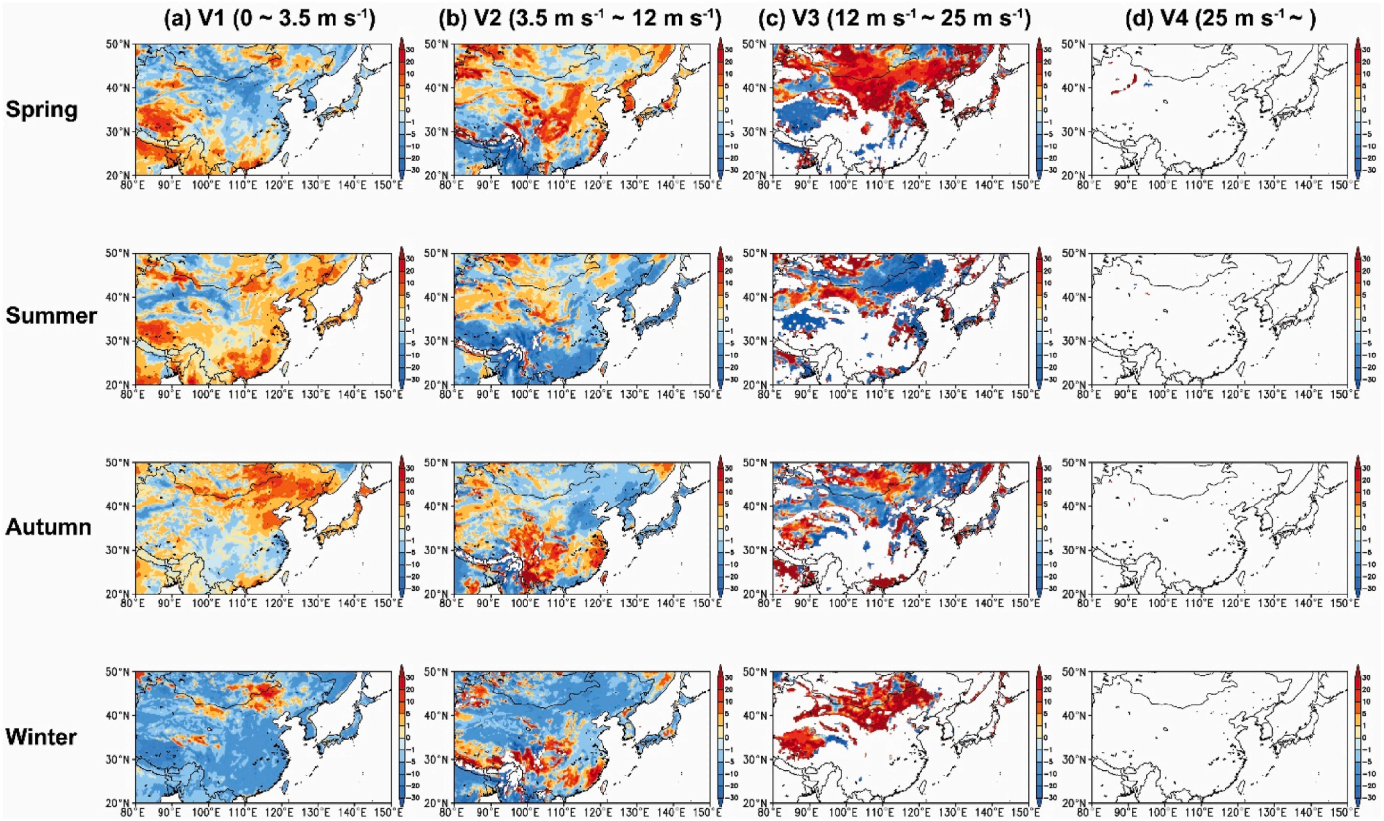

Fig. 4. The difference (unit: %) in the frequency of each wind velocity range between the second half (1999–2018) and the first half (1979–1998) of the past 40 years (1979–2018) over East Asia. (a) ***V1*** range (0 – 3.5 m s^{-1}), (b) ***V2*** range (3.5 m s^{-1} – 12 m s^{-1}), (c) ***V3*** range (12 m s^{-1} – 25 m s^{-1}), and (d) ***V4*** range (25 m s^{-1} –).

related to Wpot between the second half (1999–2018) and the first half (1979–1998) of the past 40 years (1979–2018) was investigated (Fig. 4). This was compared with the observed recent changes in seasonal Wpot shown in Fig. 2. In the spring, the recent change in the *V*1 range exhibited a decrease at high latitudes, including the northern China and southern Mongolia regions, and an increase at low latitudes. On the other hand, the *V*3 range showed a significant increase at high latitudes. These results led to a pattern of an increase at high latitudes and a decrease at low latitudes for the recent changes in East Asian Wpot, as illustrated in Fig. 2. During the summer, East Asia exhibited a pattern of decreased Wpot, primarily due to the increased *V*1 range, and the decreased *V*3 range in northern China and southern Mongolia regions. In Fig. 2, the recent changes in autumn Wpot over East Asia denote a similar increasing trend as the spring, but the distribution follows an opposite pattern, with a decrease at high latitudes and an increase at low latitudes. This is attributed to the increases in the *V*1 range at high latitudes and the *V*2 range at low latitudes. In the winter, there was a large decrease in the *V*1 range, which contributes zero value to the Wpot, across broad areas. In contrast, in these areas where the *V*1 range decreased, the contribution of the *V*2 range at low latitudes or the *V*3 range at high latitudes, which significantly contribute to Wpot calculations, increased. As a result, the winter Wpot in East Asia exhibited a substantial increase. The spatial distributions of linear regression coefficients regarding observed frequencies of each wind velocity range during the past 40 years presented in Fig. S2 showed results quite similar to the distribution in Fig. 4.

Then, the contributions (%) of *V*2 and *V*3 wind velocity ranges to East Asian Wpot climatology during the past 40 years (1979–2018) were investigated (Fig. 5). In East Asia, the contribution to the total Wpot is more than 90 % in the *V*2 range, where the amount of power generation increases according to the wind velocity. Wind velocities of the *V*3 range, which are good for wind power generation, contribute more than 40 % to the total Wpot in northern China and southern Mongolia, so these regions have relatively larger Wpot than other regions. This is especially noticeable in spring when the Wpot is large. Consequently, large–scale wind farms are currently located in these regions and are characterized by a notably high wind energy capacity factor [41].

A detailed analysis of the regional Wpot over East Asia, including the Korean peninsula and Japan, was conducted by adopting the sub–regions classification method suggested by Yu et al. [40] for China. Fig. 6 displays the 40-year seasonal climatology of Wpot for seven sub–regions in East Asia and their recent changes. The YHR region had the lowest Wpot of all regions in every season, followed by the SC region. During the spring, the NWC and NEC regions exhibited the largest Wpot among all sub–regions and all seasons. These sub–regions coincide with the area where the Wpot climatology was highest, as revealed in Fig. 2. With the exception of the NWC and YHR regions, the sub–regions presented the lowest Wpot during the summer. In the recent changes indicating the difference between the 1999–2018 mean and the 1979–1998 mean of Wpot, the Wpot increased in six sub–regions, excluding SC, during the spring. Among them, the KOR and JPN regions showed an increase of about 10 %, which was larger than that of other regions. During the winter, the Wpot increased in all seven sub–regions, while most sub–regions experienced a decrease in Wpot during the summer. The contributions of the *V*2 and *V*3 wind velocity ranges to the Wpot in seven sub–regions were examined during the past 40 years (Figs. S3 and 7). The time series of contributions of the *V*2 and *V*3 wind velocity ranges and their regression coefficients are presented in Fig. S3 and Table S1. The regression coefficients of the *V*2 and *V*3 wind velocity ranges have the same absolute values but opposite signs. Overall, the contribution trends of the *V*2 and *V*3 wind velocity ranges across all sub–regions and all seasons are very small and not statistically significant. However, in both NWC and NEC regions during winter, the *V*2 range decreased, and the *V*3 range increased at statistically significant

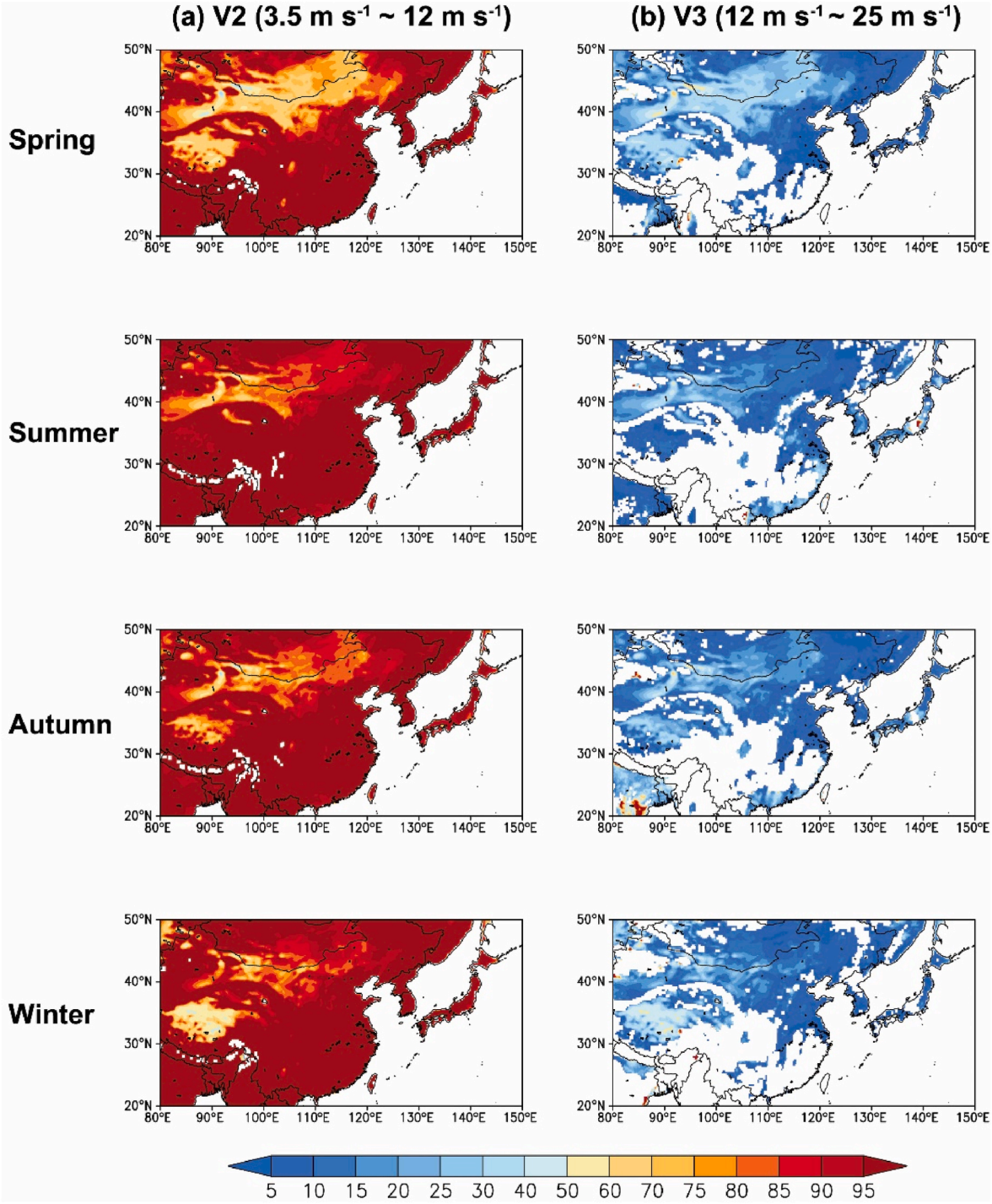

Fig. 5. The contributions (unit: %) of (a) ***V2*** (3.5 m s^{-1} – 12 m s^{-1}) and (b) ***V3*** (12 m s^{-1} – 25 m s^{-1}) wind velocity ranges to East Asian Wpot climatology during the past 40 years (1979–2018).

levels. Fig. 7 exhibits the contributions of the *V*2 and *V*3 wind velocity ranges to the 40-year seasonal climatology of Wpot. The NWC region had a high proportion of the *V*3 range to the Wpot climatology across all seasons. Specifically, during the spring, which had the highest Wpot values in East Asia, the *V*3 range contributed nearly 30 % to the Wpot climatology. In contrast, the YHR region with the lowest Wpot also had a low proportion of the *V*3 range across all seasons. Therefore, the contribution of the *V*3 range to the Wpot, which is the most favorable wind velocity range for wind power generation, had a considerable effect on leading regional differences in the Wpot.

Prior to predicting the future changes of Wpot in East Asia using multi–RCMs, the performance of individual RCMs for Wpot was evaluated. First, the bias in Wpot between RCMs and ERA5 dataset was analyzed, and compared the interannual variability and seasonal climatology of Wpot for RCMs and ERA5 dataset. It was found that RCMs underestimate observations in some regions, such as northern China and southern Mongolia regions, but overestimate in most regions (Fig. S4). Additionally, RCMs were found to overestimate the interannual variability and seasonal climatology of Wpot averaged over the East Asian domain (Figs. S5and S6). These results are attributed to the overestimation of 10 m wind velocity in the RCMs produced through the CORDEX–East Asia project, which is consistent with the findings of

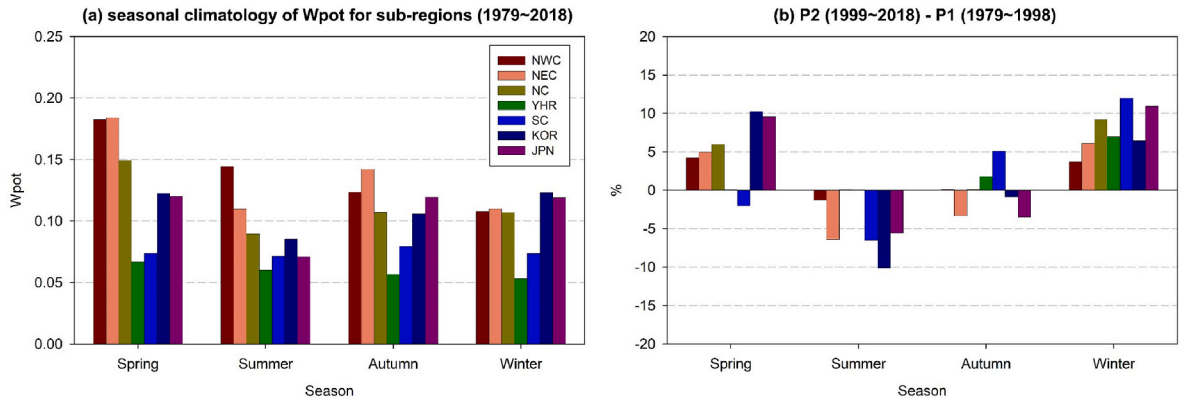

Fig. 6. The seasonal climatology of Wpot for seven sub–regions and their difference (%) between the second half (1999–2018) and the first half (1979–1998) of the past 40 years over East Asia.

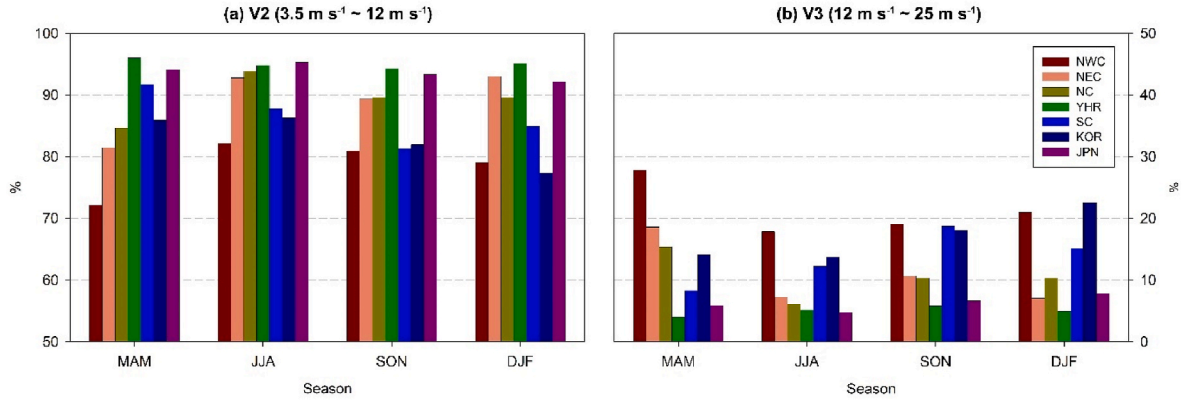

Fig. 7. The contributions (unit: %) of (a) ***V2*** (3.5 m s^{-1} – 12 m s^{-1}) and (b) ***V3*** (12 m s^{-1} – 25 m s^{-1}) wind velocity ranges to the Wpot climatology in seven sub–regions during the past 40 years (1979–2018).

previous studies targeting China [8–10]. To reduce the bias of these climate models, bias–correction techniques are sometimes applied to climate models. However, caution is required as applying bias correction techniques to downscaled climate models can add uncertainty to future climate projections, leading to decisions that are not robust across plausible climate projections [42]. Furthermore, since future projections of wind velocity and Wpot are represented using percentiles instead of raw values, bias–correction techniques were not applied to the wind velocity datasets of RCMs in this study.

Next, the Taylor diagram, which is widely used for climate model performance evaluation, was applied (Fig. 8). The distance from each *Historical* experiment to the reference (observation) indicates the model errors related to spatial patterns [43]. A reference point (red dot) denotes a perfect model performance with the same spatial variability (standard deviation) as the observation and the spatial correlation coefficient of 1.0. Here, the circles refer to RCMs forced by the HadGEM2–AO GCM, while the triangles represent RCMs forced by the MPI–ESM–LR GCM. The black circle and triangle indicate the MMEs of the RCMs forced by each GCM, and the black square represents the MME of the RCMs forced by all GCMs. In all seasons, the standard deviation of RCMs for Wpot in East Asia compared to observations ranges from 0.7 to 1.4, which is acceptable in terms of the standard deviation aspect, but the spatial correlation has a wide range of distribution from 0.33 to 0.87. Unlike other RCMs, the SNURCM forced by HadGEM2–AO and MPI–ESM–LR, shown in blue, displayed weaker correlations with observations. This suggests their lesser performance in simulating spatial patterns of the Wpot. In the previous study by Park et al. [13], which applied the same RCMs as this study, the SNURCM for the PVpot also exhibited weak correlations with observations. MMEs for these RCMs tend to exhibit relatively higher correlations and more similar standard deviations to observations compared to each individual RCM, indicating that MMEs have shorter distances from the reference point than each individual RCM. In particular, since the MME (black squares) of all RCMs forced by the two GCMs were found to have shorter distances from the reference point overall compared to the MMEs of each GCM, the MME will be applied to assess future Wpot changes over East Asia.

3.2. *Future change of RCM MMEs for the wpot over East Asia*

So far, the analyses have focused on the spatial distribution of the observed seasonal climatology for the Wpot and its recent changes using the ERA5 dataset in East Asia. Then, in this section, the expected changes in Wpot compared to the present under various emission scenarios assumed in the future were examined, as well as changes in wind velocity ranges that affect Wpot calculation. Based on the *RCP2.6* and *RCP8.5* emission scenarios, the future changes in the RCM MME of Wpot over East Asia were predicted by season for the periods of 2041–2065 (hereafter *T*1) and 2075–2099 (hereafter *T*2). Fig. 9 depicts the seasonal mean of future East Asian Wpot under different carbon emission levels for each time period. The seasonal mean of Wpot over East Asia is expected to show little difference across future periods and scenarios. It is expected that the future Wpot for the two periods area–averaged over East Asia, similar to the observed seasonal climatology for the Wpot, will have the largest values in the spring and similar values in the other seasons. Furthermore, it is projected that northern China and southern Mongolia regions will continue to be regions with large Wpot in the future. In the future projections of Wpot over East Asia by the percentage shown in Fig. 10, the areas marked with hatch patterns indicate the grids

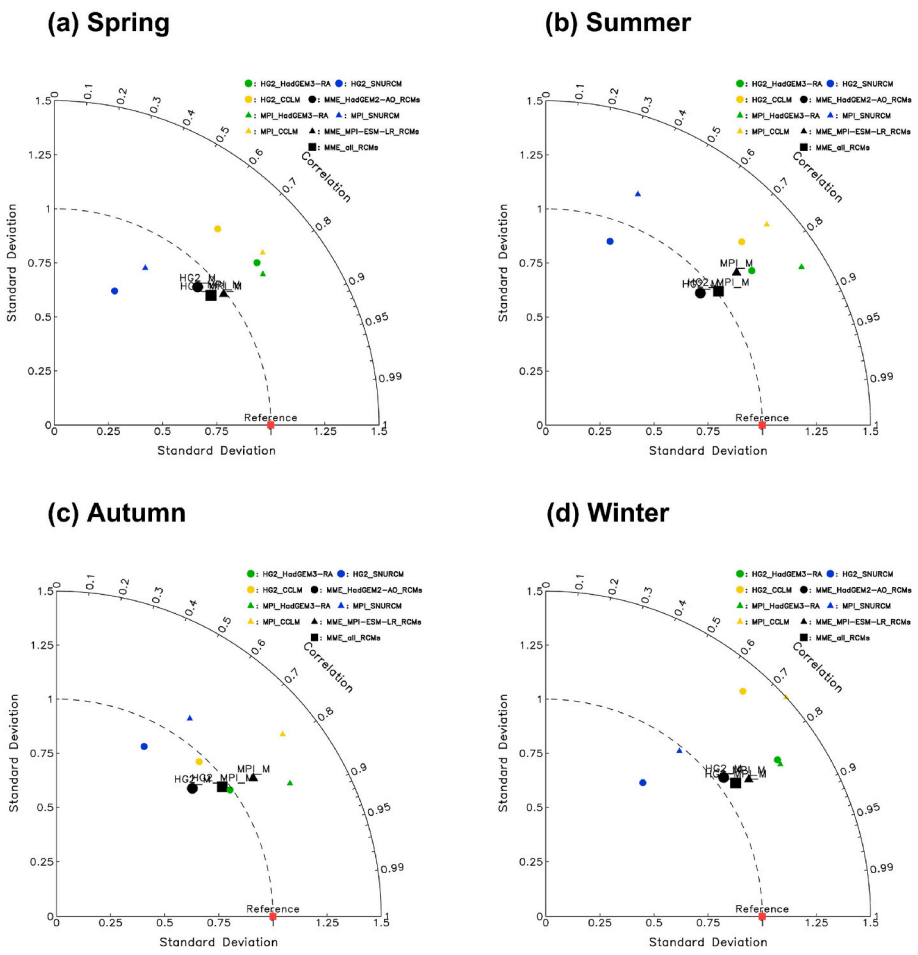

Fig. 8. Taylor diagrams of seasonal Wpot for RCMs and MMEs of the *Historical* experiment over East Asia. (a) Spring, (b) Summer, (c) Autumn, and (d) Winter. Note that HG2 and MPI refer to HadGEM2–AO GCM and MPI–ESM–LR GCM, respectively.

with good inter–RCM agreements, where at least four of the six RCMs have the same sign. Overall, the East Asian averaged Wpot will not change significantly in the future, but in a scenario with enhanced emission during the *T*2 period, the difference in projections among regions will become larger. It is projected that during the two future periods, under the *RCP8.5* scenario, an increase in Wpot in the south–central China region is expected to be prominent. According to the results of Park et al. [13], this region has also been estimated to have considerable future projections for the PVpot. However, the south–central China, as depicted in Fig. 9 of the future East Asian Wpot mean, continues to exhibit low Wpot values. Therefore, it is difficult to assess the south–central China region as a favorable region for future renewable energy production based on the results of Wpot's future projections.

The future projections (%) regarding the seasonal frequencies of each wind velocity range in relation to the future East Asian Wpot projection under different carbon emission levels for each time period were examined (Figs. S7–S10). The *V*1 range, which does not absolutely affect Wpot estimation, is expected to exhibit minimal frequency changes, ranging from −5 % to +5 %, during both future periods of all seasons in most regions under the *RCP2.6* scenario with low carbon emissions. Therefore, this indicates little significant deviation compared to the present conditions. For the *RCP8.5* scenario with the highest carbon emissions, it is predicted that the *V*1 range frequencies will exhibit a distribution similar to the *RCP2.6* scenario overall during the two future periods. However, the *V*1 range frequencies in the western regions of China will have a larger projection under the *RCP8.5* scenario compared to the *RCP2.6* scenario. Furthermore, in the comparison of the two future periods, it is expected that the values for the *T*2 period will be higher than those for the *T*1 period. Similar to the *V*1 range, the *V*4 range frequencies, which do not influence Wpot estimation, are projected to be rare in all seasons, scenarios, and future periods over East Asia. The *V*2 range, which actually contributes to Wpot, is predicted to have little change compared to the present conditions during both future periods in most regions under the *RCP2.6* scenario. However, in the summer and autumn of the *T*2 period, there will be some areas in south–central China where a slight increase is expected. Under the *RCP8.5* scenario, there will be larger regional variability compared to the *RCP2.6* scenario, which is more pronounced during the *T*2 period. Notably, it is projected that the decrease in the *V*2 range frequencies in western China will be more intensified under the *RCP8.5* scenario compared to the *RCP2.6* scenario, thereby contributing to the projected increase in *V*1 and *V*3 ranges frequencies in this region. The *V*3 range frequencies have irregular increase and decrease across all seasons, scenarios, and future periods, making it difficult to identify regional characteristics.

The contributions (%) of each wind velocity range to future seasonal Wpot mean under different carbon emission levels for the periods of *T*1 and *T*2 over East Asia were also analyzed (Figs. S11 and S12). In the distribution of contributions by each wind velocity range, it is projected that there will be minimal differences across future periods and scenarios. Consistent with the observed results (Fig. 5), the contribution of the *V*3 range to the total Wpot will remain large in northern and southwestern China and southern Mongolia. This indicates that it will continue to contribute to the large Wpot values for this region in the future, with the spring being the most prominent season in this regard.

To investigate the future changes in seasonal Wpot for sub–regions

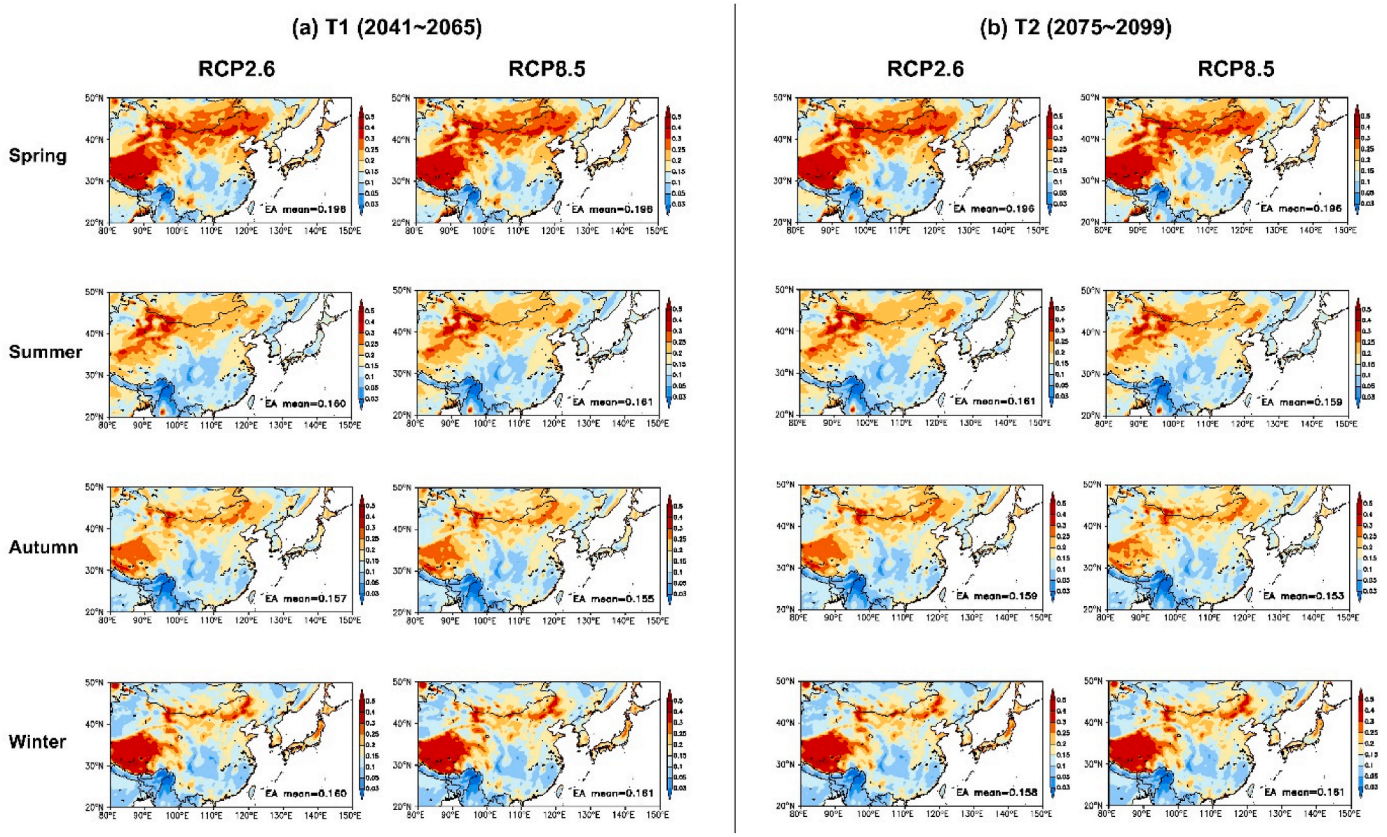

Fig. 9. The seasonal mean of future East Asian Wpot under different carbon emission levels for each time period. (a) ***T*1** (2041–2065) and (b) ***T*2** (2075–2099) periods (no unit).

over East Asia, analyses were conducted on the seasonal mean of Wpot for future scenarios and periods in seven sub–regions of East Asia (Fig. 11). As depicted in Fig. 6, representing the observed seasonal climatology of Wpot, it is projected that the YHR region will continue to have the lowest Wpot across all seasons, scenarios, and periods in the future. The NC region has a lower Wpot than the NEC region in all seasons based on observation (Fig. 6), but in the future, it is projected to have a larger or comparable Wpot than the NEC region. This seems to have resulted from the prediction in Fig. 13 that the contribution of the *V*3 range in the NC region will be larger or comparable to that in the NEC region. In the future projections of Wpot in seven sub–regions over East Asia, there will generally be minimal differences or slight changes compared to the present across all future periods and scenarios (Fig. 12). The autumn Wpot in the KOR and JPN regions will be prominently decreased under the *RCP8.5* scenario for the period of *T*2. There will be little difference in the contributions (%) of *V*2 and *V*3 wind velocity ranges to the seasonal mean Wpot in seven sub–regions, regardless of the future periods and scenarios (Fig. 13). It is predicted that the NWC region will have the highest proportion of high–quality wind velocity ranges, specifically the *V*3 range, across all seasons, scenarios, and future periods. In contrast, the YHR region is expected to have the lowest proportion. These findings suggest that the NWC region is projected to maintain the largest contribution of the *V*3 range to Wpot, while the YHR region is expected to continue having the smallest contribution in the future.

4. Summary and discussion

This study investigated the recent changes and future projections under different carbon emission levels in the Wpot over East Asia using the ERA5 datasets and the results of multi–RCMs participating in the CORDEX–East Asia phase II. Due to the constantly changing nature of wind, this study employed the wind velocity range–based Wpot estimation method in RCMs using the shortest time interval data available, which is the three–hourly wind velocity data. The observed seasonal climatology for Wpot showed that spring had the largest values overall. The northern China and southern Mongolia regions were identified as the areas with the largest values not only for PVpot but also for Wpot, and we designated these regions as a 'Hotspot' for renewable energy generation. The recent changes in Wpot showed the largest positive magnitude during the winter. This is because the frequency of the *V*1 range, which does not contribute to Wpot estimation, decreased across a wide area, while the frequencies of the *V*2 and *V*3 ranges, which contribute to the total Wpot estimation, increased. In the broad areas of East Asia, the contribution of the *V*2 wind velocity range to the total Wpot exceeded 90 %. Northern China and southern Mongolia regions had a larger Wpot compared to other regions, as the contribution of the *V*3 range, known for its optimal wind conditions in terms of wind energy generation, exceeded 40 %. This study selected seven sub–regions to examine changes in Wpot in detail by region. The YHR region had the lowest Wpot throughout all seasons. In recent Wpot changes, most sub–regions experienced an increase during winter and a decrease during summer.

The future Wpot in East Asia is expected to exhibit consistent distribution patterns across different future periods and scenarios, and the northern China and southern Mongolia regions are projected to maintain large Wpot. This is attributed to the relatively significant contribution of the *V*3 wind velocity range to the future Wpot in these regions. Overall East Asian averaged Wpot will not change significantly in both the low and the highest carbon emission scenarios compared to the present, but projection differences between regions will become larger under emission–enhanced scenarios during the *T*2 period. The YHR region is expected to continue having the lowest Wpot compared to other sub–regions, just like in the results of the past 40 years (1979–2018),

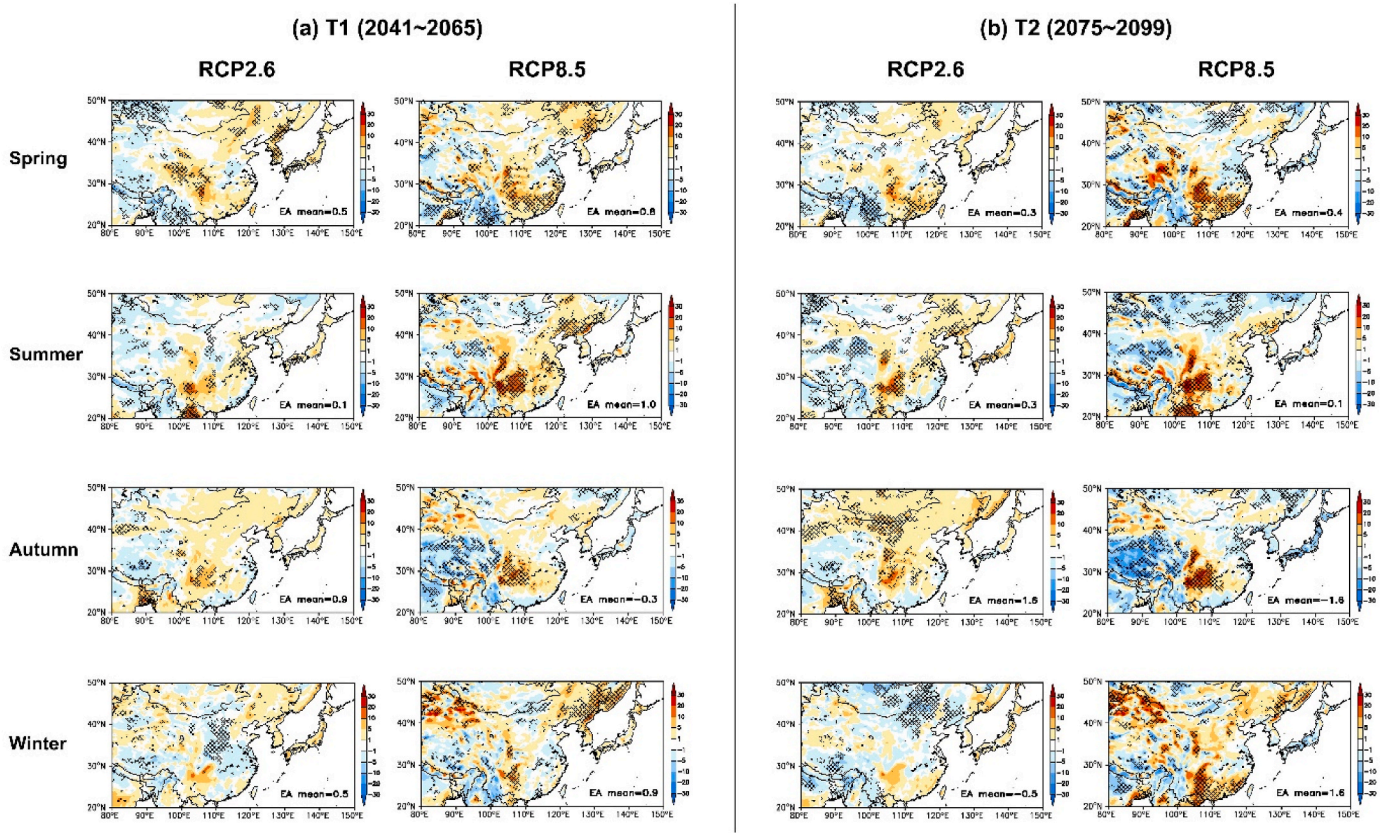

Fig. 10. The future projections (unit: %) of East Asian Wpot under different carbon emission levels for each time period. (a) ***T1*** (2041–2065) and (b) ***T2*** (2075–2099) periods. Note that the areas marked with hatch patterns indicate the grids with good inter–RCM agreements, where at least four of the six RCMs have the same sign.

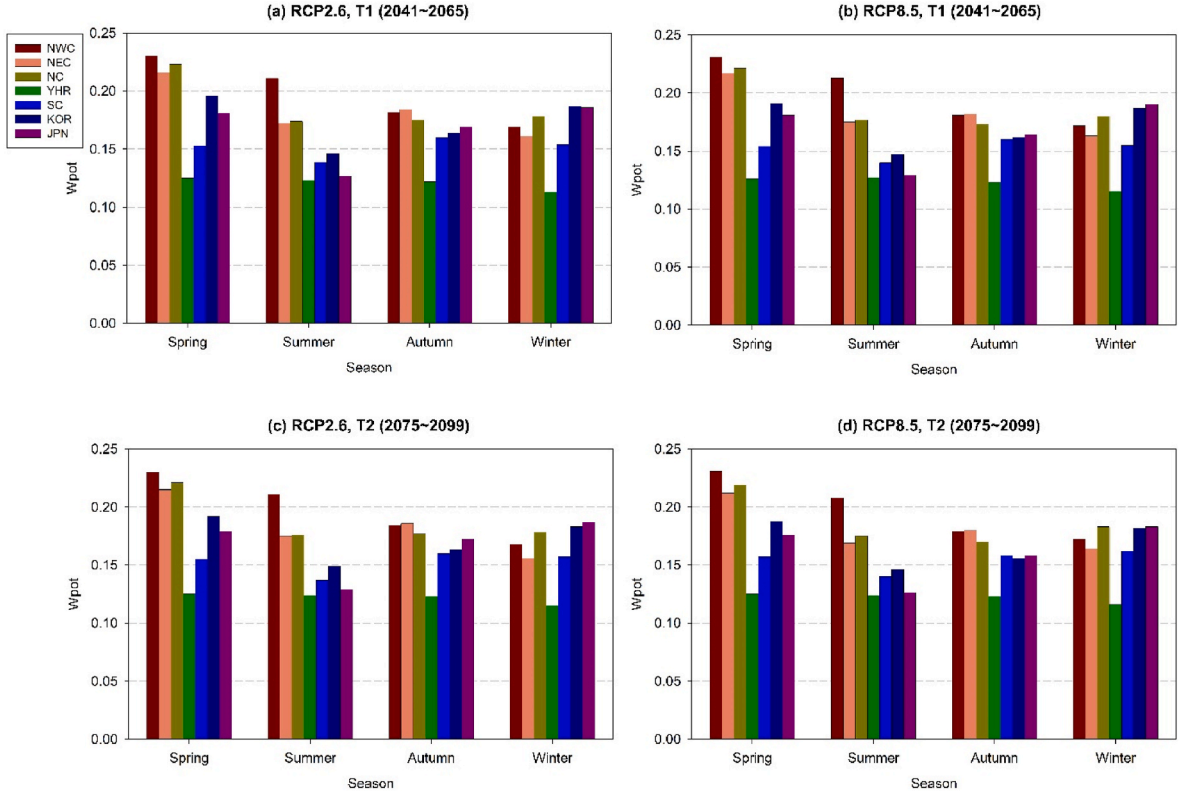

Fig. 11. The seasonal mean of Wpot for future scenarios and periods in seven sub–regions (no unit).

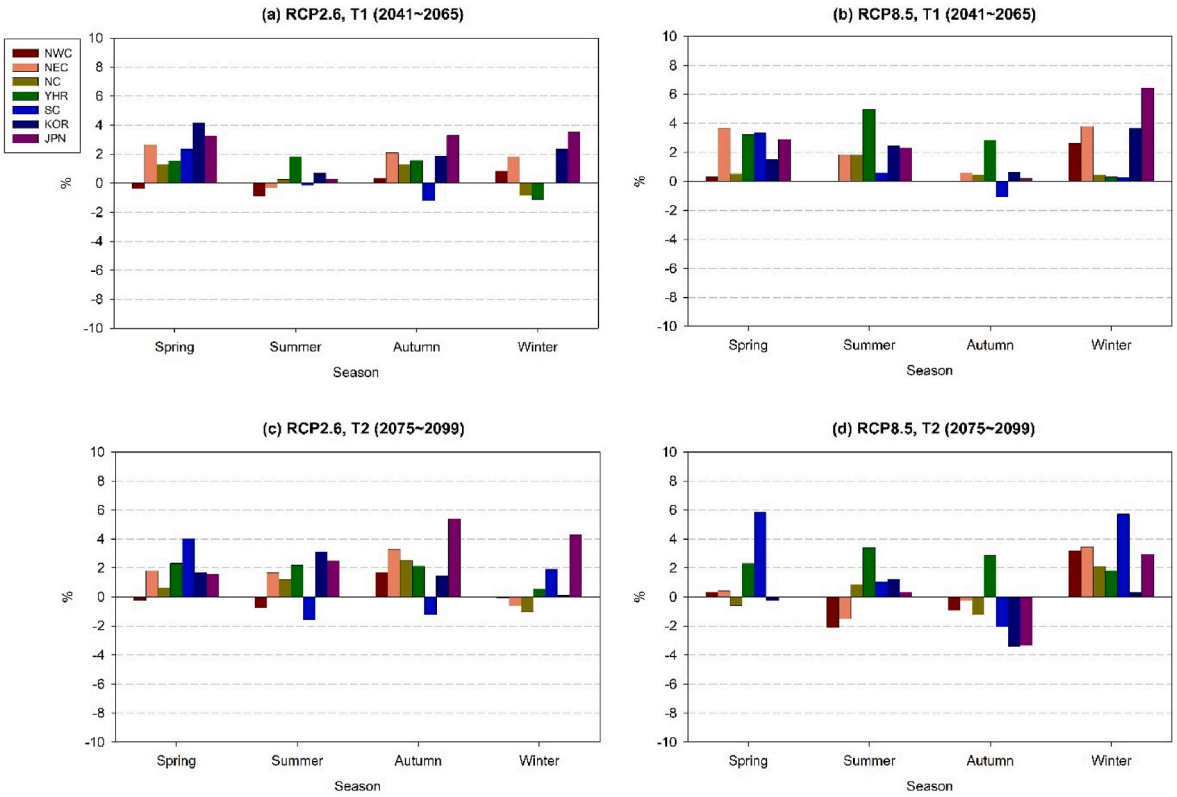

Fig. 12. The future projections (unit: %) of Wpot for future scenarios and periods in seven sub–regions.

across all seasons, scenarios, and periods in the future. The future projections of Wpot across sub–regions over East Asia will be minimal or exhibit marginal increases compared to the present, regardless of future periods and scenarios. Across all seasons, scenarios, and future periods, the NWC region is projected to exhibit the highest percentage of high–quality wind speed ranges. Conversely, the YHR region is expected to have the lowest proportion of such ranges.

This study, which projects that the average future Wpot in East Asia will not undergo significant changes in both the low and the highest carbon emission scenarios compared to the present, may not generate substantial interest among policymakers. However, considering the projected increasing regional disparities in future Wpot under intensified emission scenarios towards the end of the 21st century, this study can make a notable contribution to the optimal selection of suitable locations for wind turbine installations to enhance efficient wind energy production. The ability to derive such results was possible due to the production of dynamically downscaled high–resolution RCMs. Therefore, there is a need to enhance the use of RCMs in the renewable energy fields for future climate change adaptation and mitigation efforts. Because the site selection and exploitation of renewable energy focus more on local detailed scales rather than regional scales [10], the 25–km horizontal resolution of the six RCM simulations used in this study may not be sufficient for this purpose. Thus, for an effective response to future climate change in the renewable energy sector, there is a need for the development of climate models with more detailed spatial resolutions and their application.

Except for Mongolia, countries in East Asia, being adjacent to the ocean, have favorable conditions for harnessing offshore wind energy resources. In other words, offshore wind power, due to its offshore location, high energy output per square meter, and the ability to be built up rapidly at gigawatt–scale, offers a cost–effective means of electricity supply to densely populated coastal areas such as East Asia [44]. Furthermore, offshore wind farms have significant potential due to their ability to encounter less public resistance, access stronger and more predictable wind resources, and utilize readily available construction space [45]. In 2020, China achieved the highest capacity of new offshore wind power installations, exceeding 3 GW. China is projected to reach a total installed capacity of 200 GW for offshore wind energy by 2050 [46]. Moreover, South Korea and Japan have emerged as key markets for floating wind farms [44]. In line with this, upcoming research plans to investigate future changes in offshore Wpot over East Asia using the latest RCMs produced by the CORDEX–East Asia project team, forced by CMIP6 GCMs. Quantitative assessment of uncertainty factors in future climate projections is important in establishing climate change adaptation and mitigation strategies at the regional scale [47]. Park et al. (2023) conducted such an assessment for the temperature and precipitation variables of the RCMs produced through the CORDEX–East Asia project employed in this study [47]. The uncertainty assessment may also be applicable to future renewable energy potential calculated using climate variables from climate models. Therefore, upcoming research also plans to investigate the quantitative assessment of uncertainty in the future projections of PVpot or Wpot according to the sensitivity of multi–RCMs or scenarios to respond more effectively to climate change in the renewable energy sector. Additionally, a mechanism analysis based on atmospheric science is intended to analyze the causes of future projections for renewable energy potential.

CRediT authorship contribution statement

Changyong Park: Conceptualization, Methodology, Software, Validation, Formal analysis, Data curation, Writing – original draft, Writing – review & editing. **Seok-Woo Shin:** Software, Investigation, Data curation, Writing – review & editing. **Dong-Hyun Cha:** Conceptualization, Supervision, Funding acquisition, Writing – original draft, Writing – review & editing. **Seung-Ki Min:** Data curation, Writing – review & editing. **Young-Hwa Byun:** Data curation, Writing – review & editing. **Jin-Uk Kim:** Data curation, Writing – review & editing. **Youngeun Choi:** Data curation, Writing – review & editing.

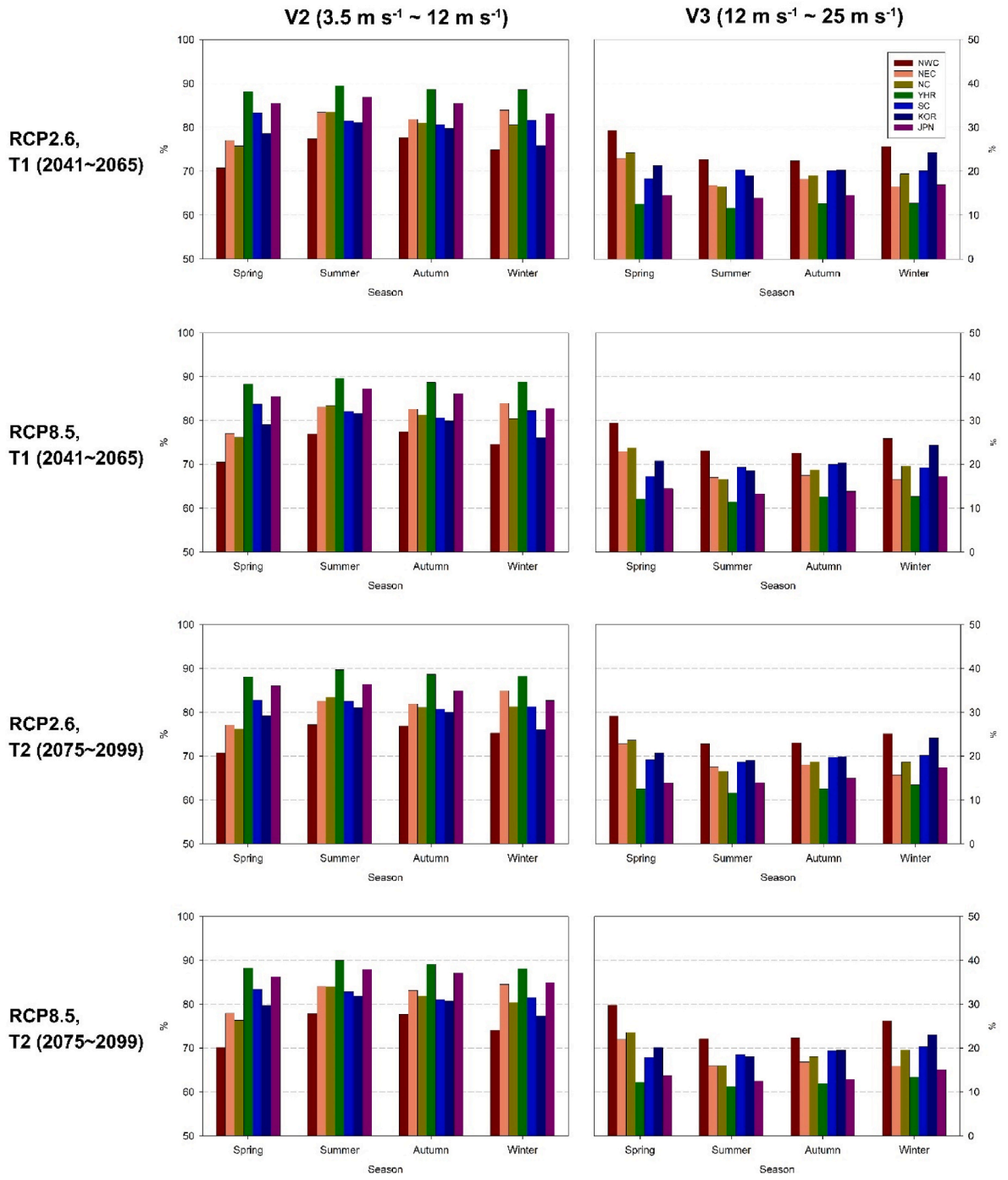

Fig. 13. The contributions (unit: %) of ***V2*** (3.5 m s^{-1} – 12 m s^{-1}) and ***V3*** (12 m s^{-1} – 25 m s^{-1}) wind velocity ranges to the seasonal mean Wpot in seven sub-regions. The left column ranges from 50 to 100 %, and the right column ranges from 0 to 50 %.

Declaration of competing interest

The authors declare that they have no known competing financial interests or personal relationships that could have appeared to influence the work reported in this paper.

Data availability

Data will be made available on request.

Acknowledgements

This work was supported by Korea Environment Industry &Technology Institute (KEITI) through "Climate Change R&D Project for New Climate Regime.", funded by Korea Ministry of Environment (MOE) (2022003560002) and in part funded by the Korea Meteorological Administration Research and Development Program under Grant RS–2024–00403386.

Appendix A. Supplementary data

Supplementary data to this article can be found online at https://doi.

org/10.1016/j.rser.2024.114747.

References

[1] BP. Bp statistical review of world energy 2021. London: BP; 2022. l.c.).
[2] RE100. RE100 annual disclosure report 2022: Driving renewables in a time of change. The Climate Group & CDP; 2023.
[3] EEA, *Europe's onshore and offshore wind energy potential.* Copenhagen: European Environment Agency; 2009.
[4] Vezzoli C, et al. Designing sustainable energy for all. Switzerland: Green Energy and Technology; 2018.
[5] Giorgi F, Jones C, Asrar GR. Addressing climate information needs at the regional level: the CORDEX framework. WMO Bull 2009;58:175e183.
[6] Ohba M. The impact of global warming on wind energy resources and ramp events in Japan. Atmosphere 2019;10:265. https://doi.org/10.3390/atmos10050265.
[7] Gao Y, Ma S, Wang T. The impact of climate change on wind power abundance and variability in China. Energy 2019;189:116215. https://doi.org/10.1016/j.energy.2019.116215.
[8] Li D, Feng J, Dosio A, Qi J, Xu Z, Yin B. Historical evaluation and future projections of 100-m wind energy potentials over CORDEX-East Asia. J Geophys Res 2020;125:e2020JD032874. https://doi.org/10.1029/2020JD032874.
[9] Li T, Liu G, Fang J, Tang J. Dynamical downscaling of inland and offshore near-surface wind speed over China in CORDEX East Asia Phase I and II experiments. Int J Climatol 2022;42:6996–7012. https://doi.org/10.1002/joc.7625.
[10] Li T, Hui P, Tang J, Fang J. Future projections of wind and solar energy resources over China from regional climate models based on bias correction. Environ. Res. Commun. 2023;5:061004. https://doi.org/10.1088/2515-7620/acddbb.
[11] Costoya X, deCastro M, Carvalho D, Feng Z, Gómez-Gesteira M. Climate change impacts on the future offshore wind energy resource in China. Renew Energy 2021;175:731–47. https://doi.org/10.1016/j.renene.2021.05.001.
[12] Chan Z, Guo J, Li W, Zhang F, Xiao C, Pan Z. Changes in wind energy potential over China using a regional climate model ensemble. Renew Sustain Energy Rev 2022;159:112219. https://doi.org/10.1016/j.rser.2022.112219.
[13] Park C, Shin S-W, Kim G, Cha D-H, Min S-K, Lee D, Byun Y-H, Kim J-U. What determines future changes in photovoltaic potential over East Asia? Renew Energy 2022;185:338–47. https://doi.org/10.1016/j.renene.2021.12.029.
[14] Zhang J, You Q, Ullah S. Changes in photovoltaic potential over China in a warmer future. Environ Res Lett 2022;17:114032. https://doi.org/10.1088/1748-9326/ac9e0b.
[15] Li T, Chen J, Zhao R, Tang J, Zuo D, Tian L, Zhang Z. Historical simulation of photovoltaic potential over China within the CORDEX-EA-II framework. Theor Appl Climatol 2023. https://doi.org/10.1007/s00704-023-04527-9.
[16] Ha S, Zhou Z, Im E-S, Lee Y-M. Comparative assessment of future solar power potential based on CMIP5 and CMIP6 multi-model ensembles. Renew Energy 2023;206:324–35. https://doi.org/10.1016/j.renene.2023.02.039.
[17] Hersbach H, et al. Global reanalysis: goodbye ERA-Interim, hello ERA5, vol. 159. ECMWF Newsletter; 2019. https://doi.org/10.21957/vf291hehd7.
[18] Liu H, Dong L, Yan R, Zhang X, Guo C, Liang S, Tu J, Feng X, Wang X. Evaluation of near-surface wind speed climatology and long-term trend over China's mainland region based on ERA5 reanalysis. Climatic and Environmental Research 2021;26:299–311. https://doi.org/10.3878/j.issn.1006-9585.2021.20101. in Chinese.
[19] Wu J, Shi Y. Changes in surface wind speed and its different grades over China during 1961–2020 based on a high-resolution dataset. Int J Climatol 2022;42:3954–67. https://doi.org/10.1002/joc.7453.
[20] Martin GM, Bellouin N, Collins WJ. The HadGEM2 family of met office Unified model climate configurations. Geosci Model Dev (GMD) 2011;4:723–57. https://doi.org/10.5194/gmd-4-723-2011.
[21] Baek HJ, et al. Climate change in the 21st century simulated by HadGEM2-AO under representative concentration pathways. Asia Pac. J. Atmos. Sci. 2013;49:603–18. https://doi.org/10.1007/s13143-013-0053-7.
[22] Sperber KR, Annamalai H, Kang IS, Kitoh A, Moise A, Turner A, Wang B, Zhou T. The Asian summer monsoon: an intercomparison of CMIP5 vs. CMIP3 simulations of the late 20th century. Clim. Dyn. 2013;41:2711–44. https://doi.org/10.1007/s00382-012-1607-6.
[23] Guo Y, Cao J, Li H, Wang J, Ding Y. Simulation of the Interface between the Indian summer monsoon and the East Asian summer monsoon: intercomparison between MPI-ESM and ECHAM5/MPI-OM. Adv Atmos Sci 2016;33:294–308. https://doi.org/10.1007/s00376-015-5073-z.
[24] Edwards JM, Slingo A. Studies with a flexible new radiation code. I: choosing a configuration for a large-scale model. Q J R Meteorol Soc 1996;122:689–719. https://doi.org/10.1002/qj.49712253107.
[25] Cusack S, Edwards JM, Crowther MJ. Investigating k distribution methods for parameterizing gaseous absorption in the Hadley Centre Climate Model. J Geophys Res 1999;104:2051–7. https://doi.org/10.1029/1998JD200063.
[26] Briegleb BP. Delta-Eddington approximation for solar radiation in the NCAR community climate model. J Geophys Res 1992;97:7603–12. https://doi.org/10.1029/92JD00291.
[27] Hack JJ, Boville BA, Briegleb BP, Kiehl JT, Williamson DL. Description of the NCAR Community climate model (CCM2) (No. NCAR/TN-382+STR). University Corporation for Atmospheric Research; 1993. https://doi.org/10.5065/D6QZ27XV.
[28] Ritter B, Geleyn JF. A comprehensive radiation scheme for numerical weather prediction models with potential applications in climate simulations. Mon Weather Rev 1992;120:303–25. https://doi.org/10.1175/1520-0493(1992)120<0303:ACRSFN>2.0.CO;2.
[29] Davies T, Cullen MJP, Malcolm AJ, Mawson MH, Staniforth A, White AA, Wood N. A new dynamical core for the met office's global and regional modeling of the atmosphere. Q J R Meteorol Soc 2005;131:1759–82. https://doi.org/10.1256/qj.04.101.
[30] Cha DH, Lee DK. Reduction of systematic errors in regional climate simulations of the summer monsoon over East Asia and the western North Pacific by applying the spectral nudging technique. J Geophys Res 2009;114:D14108. https://doi.org/10.1029/2008JD011176.
[31] Rockel B, Will A, Hense A. The regional climate model COSMO-CLM(CCLM). Meteorol Z 2008;17:347–8. https://doi.org/10.1127/0941-2948/2008/0309.
[32] Manwell JF, McGowan JG, Rogers AL. Wind energy Explained: Theory, Design and application. Chichester: John Wiley & Sons; 2009.
[33] Elliott DL. *Adjustment and analysis of data for regional wind energy assessments,*. Workshop on Wind Climate. Asheville: North Carolina; 1979.
[34] Tobin I, et al. Climate change impacts on the power generation potential of a European mid-century wind farms scenario. Environ Res Lett 2016;11:034013. https://doi.org/10.1088/1748-9326/11/3/034013.
[35] Mathew S. Wind energy: fundamentals, resource analysis and economics. Berlin and Heidelberg: Springer-Verlag; 2006.
[36] Jerez S, Trigo RM. Time-scale and extent at which large-scale circulation modes determine the wind and solar potential in the Iberian Peninsula. 2013, 044035. https://doi.org/10.1088/1748-9326/8/4/044035. 8.
[37] Jerez S, Trigo RM, Sarsa A, Lorente-Plazas R, Pozo-Vázquez D, Montávez JP. Spatio-temporal complementarity between solar and wind power in the Iberian Peninsula. Energy Proc 2013;40:48–57. https://doi.org/10.1016/j.egypro.2013.08.007.
[38] Jerez S, Thais F, Tobin I, Wild M, Colette A, Yiou P, Vautard R. The CLIMIX model: a tool to create and evaluate spatially-resolved scenarios of photovoltaic and wind power development. Renew Sustain Energy Rev 2015;42:1–15. https://doi.org/10.1016/j.rser.2014.09.041.
[39] Ravestein P, van der Schrier G, Haarsma R, Scheele R, van den Broek M. Vulnerability of European intermittent renewable energy supply to climate change and climate variability. Renew Sustain Energy Rev 2018;97:497–508. https://doi.org/10.1016/j.rser.2018.08.057.
[40] Yu K, Hui P, Zhou W, Tang J. Evaluation of multi-RCM high-resolution hindcast over the CORDEX East Asia Phase II region: mean, annual cycle and interannual variations, vol. 40; 2020. p. 2134–52. https://doi.org/10.1002/joc.6323.
[41] Sherman P, Chen X, McElroy MB. Wind-generated electricity in China: decreasing potential, interannual variability and association with changing climate. Sci Rep 2017;7:16294. https://doi.org/10.1038/s41598-017-16073-2.
[42] Lafferty DC, Sriver RL. Downscaling and bias-correction contribute considerable uncertainty to local climate projections in CMIP6. npj Clim. Atmos. Sci. 2023;6:158. https://doi.org/10.1038/s41612-023-00486-0.
[43] Taylor KE. Summarizing multiple aspects of model performance in a single diagram. J Geophys Res 2001;106:7183–92. https://doi.org/10.1029/2000JD900719.
[44] IRENA. Offshore renewables: an action agenda for deployment. Abu Dhabi: International Renewable Energy Agency; 2021.
[45] UN.ESCAP. Low carbon green growth roadmap for Asia and the Pacific : turning resource constraints and the climate crisis into economic growth opportunities. 2012 (Bangkok: UN.ESCAP).
[46] Wang Z, et al. Technology roadmap: China wind energy development roadmap 2050. Paris and Beijing: International Energy Agency and Energy Research Institute; 2011.
[47] Park C, et al. Uncertainty assessment of future climate change using bias-corrected high-resolution multi-regional climate model datasets over East Asia. Clim. Dyn. 2024;62:1983–96. https://doi.org/10.1007/s00382-023-07006-z.